

Article

# Effect of Modified Hexagonal Boron Nitride Nanoparticles on the Emulsion Stability, Viscosity and Electrochemical Behavior of Nanostructured Acrylic Coatings for the Corrosion Protection of AISI 304 Stainless Steel

Alma P. Ysiwata-Rivera <sup>1</sup>, Ernesto Hernández-Hernández <sup>1</sup>, Gregorio Cadenas-Pliego <sup>1</sup> , Carlos A. Ávila-Orta <sup>1</sup> , Pablo González-Morones <sup>1</sup>, Juan A. Velásquez-de Jesús <sup>1</sup>, Edgar Cuara-Díaz <sup>1</sup>, Carlos A. Gallardo-Vega <sup>1</sup> and José M. Mata-Padilla <sup>1,2,\*</sup> 

<sup>1</sup> Centro de Investigación en Química Aplicada, Blvd. Enrique Reyna Hermsillo No. 140, C.P., Saltillo 25294, Mexico; almaysiwata\_26@hotmail.com (A.P.Y.-R.); ernesto.hernandez@ciqa.edu.mx (E.H.-H.); gregorio.cadenas@ciqa.edu.mx (G.C.-P.); carlos.avila@ciqa.edu.mx (C.A.Á.-O.); pablo.gonzalez@ciqa.edu.mx (P.G.-M.); arturo\_beuc@hotmail.com (J.A.V.-d.J.); edgar.cuara@ciqa.edu.mx (E.C.-D.); carlos.gallardo@ciqa.edu.mx (C.A.G.-V.)

<sup>2</sup> Consejo Nacional de Ciencia y Tecnología-Centro de Investigación en Química Aplicada (CIQA), Blvd. Ing. Enrique Reyna Hermsillo No. 140, C.P., Saltillo 25294, Mexico

\* Correspondence: jose.mata@ciqa.edu.mx or jmmata@conacyt.mx; Tel.: +52-844-438-9830 (ext. 1246)

Received: 15 April 2020; Accepted: 6 May 2020; Published: 19 May 2020



**Abstract:** In this study, the effect of pure and modified hexagonal boron nitride (h-BN) nanosheet incorporation on the stability, viscosity, and electrochemical behavior of a waterborne emulsion acrylic coating was studied. The functionalization of h-BN nanoplatelets with polyacrylic acid (PAA) plasma polymerization was performed, and the successful surface modification was determined through water dispersion testing, Fourier transform infrared spectroscopy and thermogravimetric analysis, X-ray photoelectron spectroscopy, and also by transmission electronic microscopy. Later, the stability and viscosity properties of emulsion nanostructured acrylic coatings, which were previously prepared by an ultrasound-assisted mixing system, were analyzed using zeta potential and rheometry testing, respectively. The electrochemical behavior was analyzed by electrochemical impedance spectroscopy. The results prove an effective deposition of PAA films on the h-BN surfaces, which enhanced the stability and viscosity acrylic of nanostructured coatings due to the interactions between the h-BN nanoplatelets surface and emulsion acrylic paint and also with the thickener additives. On the other hand, the electrochemical analysis demonstrated a significant increase (two orders of magnitude) in corrosion resistance in the acrylic nanostructured coatings with 1 wt.% of unmodified and modified h-BN nanoplatelets concerning pure acrylic paint due to a barrier protection mechanism of corrosion inhibition. Therefore, the results demonstrate that the surface modification of h-BN by plasma polymerization (green technology) helped to solve the low dispersibility issue of BN nanosheet surfaces in a waterborne polymer matrix to obtained green nanostructured acrylic coatings with the right balance in in-can properties and corrosion inhibition of AISI 304 stainless steel.

**Keywords:** nanocomposite coatings; hexagonal boron nitride; corrosion resistance; impedance spectroscopy

## 1. Introduction

Corrosion is one of the main problems related to the deterioration of all the steel-made metallic components, and this carries to repair or replace involving in a significant impact on society [1]. In this sense, the National Association of Corrosion Engineers (NACE) reported that, in 2013, the global economic loss due to corrosion was estimated to be USD 2.5 trillion [2]. In this regard, it is necessary to find more robust solutions to prevent the phenomenon of oxidation and corrosion that deteriorate steel parts exposed mainly to elevated temperatures or marine environments. One of the most decisive option to deal with corrosion problems is developing protective coatings of proper materials on the steel surface with improved corrosion and oxidation resistance [3].

Over time, corrosion protection coatings have been developed with constituents such as hexavalent chromium [4], tributyltin [5], cadmium [6], cobalt [7] and copper [8] and used in different marine devices and maritime transports. However, these compounds have been recently classified as toxic for the marine eco-system and carcinogenic to humans [3,9]. From this perspective, the coating industry is interested to find more environmentally friendly substitutes with greater efficiency and lower cost for these commercial but hazardous coating constituents [9].

Acrylic resins have become an attractive alternative in protective coatings because of its significant advantages, including weathering durability, optical clarity, chemical stability, excellent adhesion, and low cost [10]. Besides, water-borne acrylic coatings are an environmentally friendly option because they contain low levels of volatile organic compounds (VOCs) [11], which make them promising candidates to replace the coatings based on hazardous constituents. However, water-borne coatings present some disadvantages when they are applied due to the low solids content and the low rate of evaporation of water, and when they are in storage by the dispersion stability that could impact the product lifetime [11–14]. Some of these issues could be improved by the implementation of nanotechnology advances for the development of organic coatings.

Nowadays, nanotechnology is consolidating as one of the critical technologies of the future. The main interest has been focused on polymer-based nanocomposites with diverse nanoparticles [15–18]. Furthermore, the addition of nanoparticles can have beneficial effects on the anticorrosive and mechanical properties of organic coatings, even at low loads because of the inherent small sizes and the particle morphologies. One of the most critical challenges to study is the asset interface nanoparticle-polymer host resin and the way to improve their interfacial interactions [19]. These studies have been focused on the improvement of its anticorrosive properties, keeping in mind the mechanisms of inhibition of the traditionally reported corrosion phenomenon, such as (1) barrier protection, (2) cathodic protection, and (3) anodic passivation [19,20]. In this sense, the incorporation of modified or unmodified laminar nanoparticles, such as graphene or hexagonal boron nitride (h-BN) has enhanced the corrosion protection behavior of the polymeric coating [3,21–24].

Mainly, the h-BN is a laminar nanoparticle that has exceptional physics and chemical properties, such as low density, high hardness, good oxidation resistance, and outstanding barrier property [23,24], which make it an excellent anticorrosive constituent for polymer nanocomposite. Husain et al. found that the incorporation of h-BN into polyvinyl alcohol (PVA) improved the anticorrosive protection of stainless steel under simulated marine environments conditions. This behavior was attributed to the hydrophobic, inert, and dielectric nature of the h-BN [25]. On the one hand, Cui et al. introduced h-BN into epoxy resin and enhanced corrosion protection. The reason for this improvement was that the existence of dispersed h-BN effectively interrupted the crack propagation and reduced the coating porosity, thus inhibiting the penetration of corrosive medium in epoxy resin [3,23].

An interesting aspect in the case of nanocomposite coatings is that when incorporating pristine or modified nanoparticles to polymer resin, it is possible to generate coatings with enhanced properties, especially anticorrosive activity and different anticorrosion mechanisms in the same formulation. An important aspect to be considered is that the increase in interfacial interaction between the nanoparticles and the coating matrix is strongly affected by the chemical compatibility between the two phases and the dispersion and distribution of the nanoparticles within the polymer matrix. The surface

modification of the nanoparticles can directly affect this interaction, modifying the anticorrosive properties of the nanocomposite coatings.

One of the most promising technologies for the surface modification of nanoparticles has been the plasma polymerization due the fact that it is simple, fast, dry, and free of organic solvents. For example, this technology has been used in our research group for modifying different nanoparticles, such as carbon nanofibers, graphene, clay, copper, and titanium oxide with several monomers (e.g., ethylene, acrylic acid, methyl methacrylate, etc.) [26–32], to mainly improve the dispersion and compatibility between the nanoparticles and a polymer matrix.

Therefore, the main aim of this study is to understand the effect of surface modification of hexagonal boron nitride (h-BN), by the solvent-free plasma polymerization (green technology), on the stability and viscosity of waterborne acrylic coating (green coating) and its posterior influence on its corrosion protection efficiency and mechanism on 304 stainless steel substrates. The surface modification of nanoparticles was analyzed by Fourier transform infrared spectroscopy (FTIR), thermogravimetric analysis (TGA), X-ray photoelectron spectroscopy (XPS), and transmission electron microscopy (TEM), while the aqueous coatings were characterized by zeta potential and apparent viscosity behavior. The electrochemical behavior of the acrylic nanostructured coatings deposited on 304 stainless steel substrates was studied using electrochemical impedance spectroscopy (EIS).

## 2. Materials and Methods

### 2.1. Materials

In the present study, h-BN nanoplatelets with a purity of 99%, an average size of 70 nm and a density of 2.29 g/cm<sup>3</sup> were purchased from Lower Friction (M. K. Impex, Mississauga, ON, Canada). Acrylic acid (AA) monomer with a purity of 99% and an Mw of 77.02 kg/mol was acquired from Sigma-Aldrich (St Louis, MO, USA), a commercial water-based acrylic resin with a density of 1.02–1.04 g/cm<sup>3</sup> and pH 8–10 was purchase from Berel (Santa Catarina, Nuevo Leon, Mexico) and a surfactant Eumulgin W-1000 was purchased from Henkel Mexicana (Huixquilucan, Estado de Mexico, Mexico). The substrates used for the purpose of coating were 304 stainless steel (SS-304) with the next chemical composition (C: 0.06%, Cr: 17.87%, Ni: 7.70%, Mn: 1.05%, Cu: 0.20%, Si: 0.035%, N: 0.045%, P: 0.025% and S: 0.001%) and were cut to a dimension of 50 mm × 50 mm × 1 mm and 25 mm × 25 mm × 1 mm for corrosion studies and mechanical tests, respectively.

### 2.2. Methods and Characterization

#### 2.2.1. Surface Modification of Nanoparticles

The surface modification process was carried out into a plasma reactor, as previously reported [22,25,27]. It consisted mainly of a power controller coupled to a radiofrequency generator of 13.56 MHz, a vacuum pump, a gas flux control valve, and a 250 mL Erlenmeyer flask held over a magnetic stirring rack. The deposition of polyacrylic acid (PAA) onto the h-BN was achieved as follows: 1.1 g of nanoparticles was introduced in the Erlenmeyer flask under vacuum conditions. The initial internal pressure was 30 Pa. AA monomer flow was fixed to maintain a constant pressure of 45 Pa. The h-BN was treated for 30 min with 50 W of plasma power, maintaining a constant agitation during the exposure of the particles to the plasma.

The untreated and plasma-treated nanoparticles were tested for dispersion in water as follows: 1 mg was immersed in 10 mL of solvent and sonicated for 10 min. After a given time, photographs were taken, and the degree of dispersion, which indirectly indicated the degree of the h-BN modification, was established. Infrared spectroscopy by Fourier transform (FTIR) analysis, to determine the functional groups on h-BN after the treatment, was carried out in a Nicolet™ iS™ 5 spectrometer (Thermo Scientific, Madison, WI, USA) using the attenuated total reflectance technique (ATR). The spectra were obtained at 100 scans and a resolution of 4 cm<sup>-1</sup> between 400 and 4000 cm<sup>-1</sup> with automatic

atmosphere suppression. The thermogravimetric analysis (TGA) was used to determine the thermal stability of unmodified and modified nanoparticles, using a thermo-analyzer TA Q500. TGA curves were obtained according to the following conditions: temperature range of 30 to 600 °C, a heating rate of 10 °C/min, and an atmosphere of N<sub>2</sub>. Transmission electron microscopy (TEM) morphology analysis was performed in an equipment model FEI-TITAN 80–300 KV (Thermo Fisher Scientific, Waltham, MA, USA) with a field emission gun microscope. Aiming to understand the chemical interactions produced by the plasma treatment in the nanoparticles, the samples were analyzed by X-ray photoelectron spectroscopy (XPS) in a PHI 5000 Versa Probe II spectrometer (Physical Electronics, Inc., Chanhassen, MN, USA). The analysis consisted of obtaining the spectra in an energy scan of 0–1400 eV to quantify the chemical elements present in the surface; the samples were bombarded by a monochromatic aluminum X-ray source (Al K $\alpha$ ) with an energy of 1486.6 eV.

### 2.2.2. Preparation of Acrylic Nanostructured Coatings

The formulation procedure of the nanostructured coatings consisted of the incorporation of unmodified and modified nanoparticles into a commercial waterborne acrylic resin, with 0.1 wt.%, 0.5 wt.%, and 1 wt.% of h-BN. As a first step, the nanoparticles were dispersed in a mixture of water and a certain amount of Eumulgin W-1000 surfactant using an ultrasound bath for 10 min; then, this aqueous dispersion was incorporated into the acrylic resin. The mixture was exposed to mechanical agitation for 30 min at 250 rpm. After that, each mixture was stirred in an ultrasound semi-continuous system for 30 min.

The zeta potential is an effective way to evaluate the electrostatic behavior of the system since it indicates changes in the potential of the surface and in the forces of repulsion/attraction between particles. This potential value was determined in a Microtrac Zeta-Check potential analyzer (Microtrac-MRB, Osaka, Japan) that has a cylindrical polytetrafluoroethylene (PTFE) beaker with a capacity of 1–10 mL and an oscillating displacement piston to agitate and push the sample towards the electrodes and thus determine the level of electrostatic repulsion between the particles. The viscosity behavior of the formulations was studied in an Physica MCR-501 oscillating rheometer (Anton Paar, Graz, Austria) with a cone-plate measurement system of 50 mm diameter and a 2° angle, the choice of geometry was based on the viscosity of the sample. All measurements were carried out at shear rates of 0.001 to 1000 s<sup>-1</sup> at a temperature of 25 ± 0.05 °C with 20 measurements every 10 s.

### 2.2.3. Substrate Preparation and Deposition

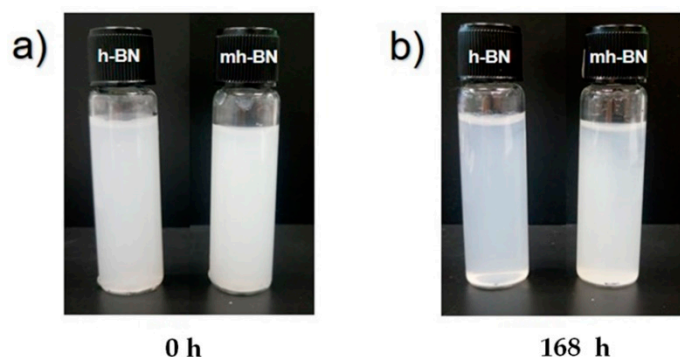
The steel substrates were polished with silicon carbide abrasive paper (SiC), cleaned in an ultrasound bath with deionized water, degreased with ethanol and acetone, and dried for further use. Subsequently, the coatings were deposited by spray coating. In this procedure, the substrates were sprayed with a high-volume low pressure (HVLP) spray gun with the prepared formulations and dried in an oven at a temperature of 50 °C for 30 min. This process was repeated again to generate a dry film of homogeneous coating with a thickness of 70 ± 10 µm.

The electrochemical measurements were carried out in a conventional three-electrode flat cell using an Autolab PGSTAT204 electrochemical system (Metrohm, Herisau, Switzerland) to evaluate the corrosion behavior of the coatings. The coated 304-SS was used as a working electrode, and the test cell included an Ag/AgCl reference electrode and a 316 stainless steel auxiliary electrode. The samples were immersed in 3.5 wt.% NaCl solution for 2 h to establish a steady open circuit potential (OCP) before the measurements. Electrochemical impedance tests were performed at the OCP over a frequency range of 100 kHz and 100 mHz, with applied 10 mV sinusoidal perturbations. NOVA 2.1 software was used for analyzing the EIS results.

### 3. Results and Discussion

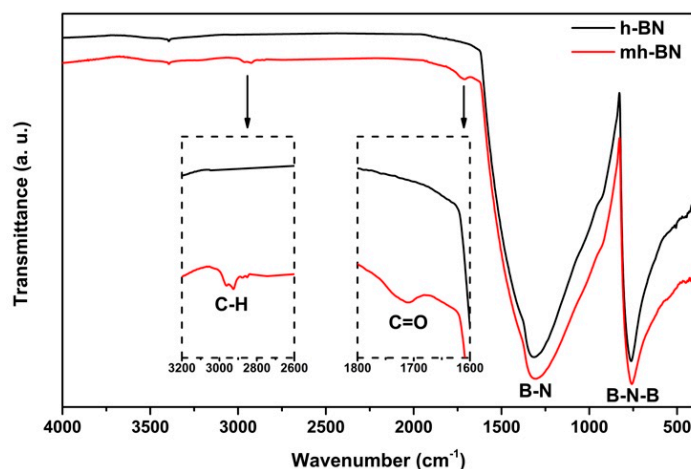
#### 3.1. Surface Modification of h-BN Nanoparticles with Plasma Functionalization

Figure 1 shows the comparison of the dispersion stability of unmodified (h-BN) and plasma-modified (mh-BN) nanoparticles at different times of storage in water. It could be seen that after the sonication of nanoparticles, both samples were suspended in the aqueous solution, despite being a hydrophobic material. This behavior is due to the exfoliation of h-BN sheets, basically by the hydrolysis during sonication, which provides the capacity to be dispersed in water, even without any surfactant or organic functionalization [33,34]. On the other hand, after standing for 168 h, the agglomerates and precipitation of the dispersion of h-BN could be found, whereas the dispersion of mh-BN was stable, and no visible precipitation was observed. This behavior was attributed to the hydroxyl and carbonyl functional groups corresponding to PAA that were deposited on the surface of the particles and resulting in a better interaction with water molecules.



**Figure 1.** Dispersions of unmodified (h-BN) and plasma-modified (mh-BN) nanoparticles in water: (a) initially and (b) after 168 h standing.

The results of the FTIR analysis of unmodified and plasma-modified h-BN are shown in Figure 2. The spectra for both samples presented two strong characteristic peaks located at 1370 and 776  $\text{cm}^{-1}$ . The peak at 1370  $\text{cm}^{-1}$  has been assigned to the in-plane B–N stretching vibration of the  $sp^2$ -bonded h-BN, while the one at 776  $\text{cm}^{-1}$  is associated with the B–N–B out-of-plane bending vibrations [35–37]. In the case of mh-BN, spectra showed the presence of two additional signals at 1712 and 2800–3000  $\text{cm}^{-1}$ , which were attributed to stretching vibrations of C=O and  $\text{CH}_2/\text{CH}$  groups related to PAA, respectively [30,38].



**Figure 2.** Infrared spectra of unmodified (h-BN) and plasma-modified (mh-BN) nanoparticles.

The thermal decomposition behavior of the organic film deposited by plasma was measured through the weight loss, as depicted in Figure 3. The thermogram of h-BN suggested a typical thermal decomposition behavior and a marginal weight loss of 0.49 wt.% at a temperature of 600 °C, attributable to the loss of humidity. mh-BN showed a weight loss of 3.84 wt.%, which was associated with the decomposition (chain scission reaction of the PAA chains and the degradation of the PAA chains into monomers) of the organic film deposited on the surface of h-BN [38–40].

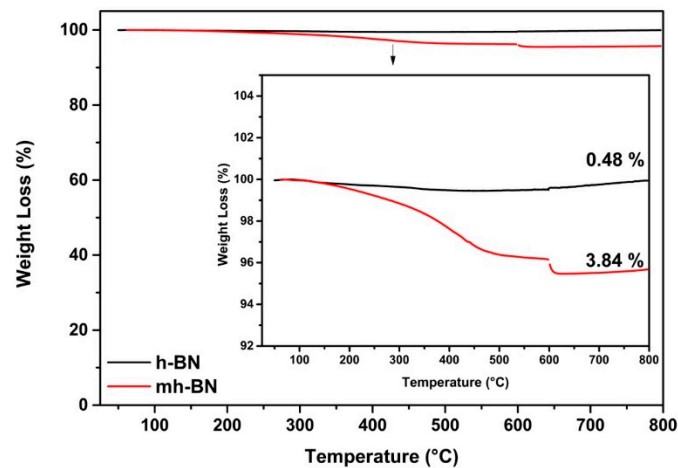


**Figure 3.** Thermogravimetric analysis (TGA) thermograms of unmodified (h-BN) and plasma-modified (mh-BN) nanoparticles.

The high-resolution transmission electron microscopy (HR-TEM) images shown in Figure 4 correspond to unmodified and plasma-modified nanoparticles. Figure 4a presents the micrograph of h-BN, where the nanoparticle shows an irregular surface, possibly due to its synthesis method. In Figure 4b the micrograph of mh-BN is shown, where a thin surface layer can be noticed on the edge of h-BN50, which corresponds to a thin polyacrylic acid layer deposited via plasma treatment. The thickness of this heterogeneous superficial nanolayer was less than 5 nm.

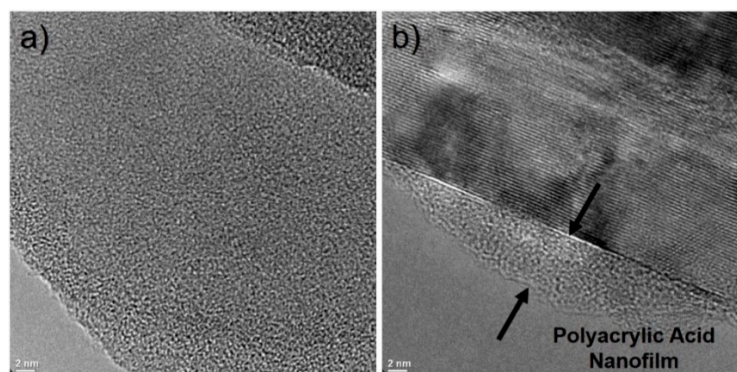


**Figure 4.** HR-TEM micrographs of: (a) unmodified (h-BN) and (b) plasma-modified (mh-BN) nanoparticles.

Furthermore, XPS was used to investigate the chemical surface of unmodified and plasma-modified nanoparticles. Figure 5a shows the XPS survey spectrums obtained for both samples, which consisted mainly of nitrogen (N 1s), boron (B 1s), oxygen (O 1s) and carbon (C 1s), with peaks corresponding to bonding energies of 398.5, 190.8, 284.8, 534.9 eV, respectively. These values are consistent with the values reported for h-BN [41,42]. The additional oxygen and carbon from h-BN could result from the exposure of nanoparticles to air before the XPS measurement, while for h-BN50 the intensity of these peaks was increased due to the plasma polyacrylic acid deposited during the treatment.

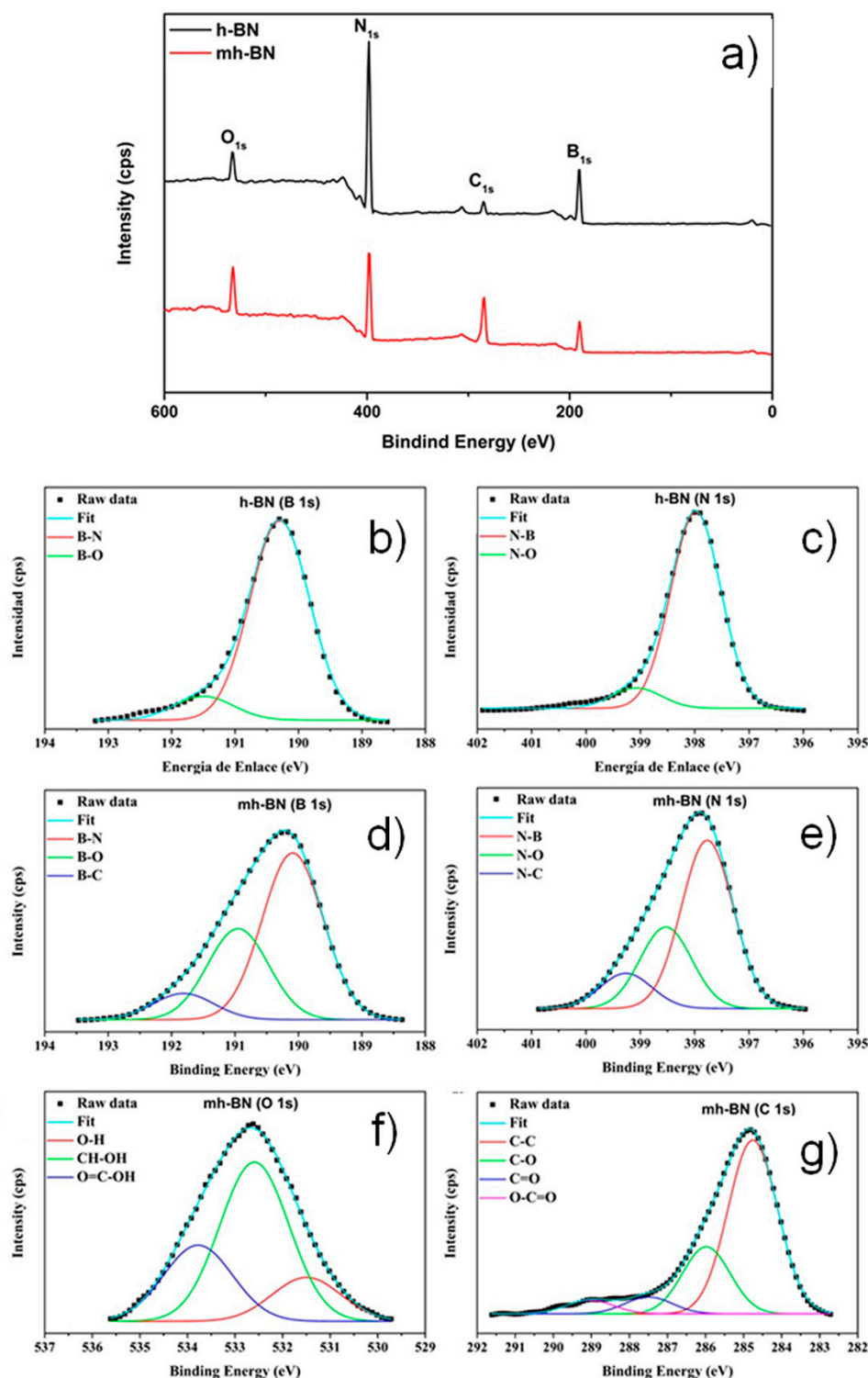


**Figure 5.** (a) X-ray photoelectron spectroscopy (XPS) survey spectra of unmodified (h-BN) and plasma-modified (mh-BN) nanoparticles, and the high-resolution XPS spectra of: (b) B 1s and (c) N 1s from h-BN; (d) B 1s, (e) N 1s, (f) O 1s; and (g) C 1s from mh-BN.

Figure 5b–g presents the high-resolution XPS spectra of B 1s, N 1s, O 1s, and C 1s, which unravel the chemical state structure of h-BN and h-BN50. The B 1s spectrum of the h-BN (Figure 5b) can be fitted by two curves, associated to B–N and B–O bindings energies located at 190.3 and 191.5 eV, respectively. The N 1s spectrum of h-BN (Figure 5c) can be fitted by two curves, associated to N–B

and N–O bindings located at 398.0 and 399.0 eV, respectively. These energy values are similar to those previously reported in other studies [43–47].

On the other hand, Figure 5d shows the B 1s spectrum of h-BN50, where the signals of B–N and B–O are appreciated detected and a new one at 191.9 eV associated with the B–C bond, where the carbon comes from the PAA coating. During plasma treatment, the reactive species (electrons, free radical ions, etc.) of the plasma attack the surface of the nanoparticles by breaking the B–N bonds to increase B–O and form B–C bindings [43,48]. Figure 5e presents the N 1s spectrum of mh-BN and shows the signals of N–B and N–O and a new one at 399.1 eV associated with the N–C bond. Besides, the high-resolution spectra of O 1s and C 1s of mh-BN are shown in Figure 5f,g. The O 1s spectrum showed peaks at binding energies of 531.5, 532.6, and 533.8 eV associated with O–H, CH–OH, and O=C–OH, respectively. The spectrum of C 1s was deconvolved in four peaks associated with the following chemical groups, where R can be C or H: C–C (284.8 eV), C–O (286 eV), C=O/O–C–O (287.5 eV) and CO<sub>2</sub>–R (289 eV). These energy values coincide with those previously reported in other studies [25,49–51]. The analysis by XPS clearly shows the presence of functional groups deposited on the surface of the h-BN nanoparticles, and particularly the formation of the B–C and N–C bond was observed, possibly indicating that some PAA molecules may be chemically interacting with h-BN, forming covalent bonds.

Table 1 shows the atomic percentage of B, N, O, and C in each of the samples measured. The content of both carbon and oxygen increased from 5.3 at.% (h-BN) to 11.7 at.% (h-BN50) and 5.9 at.% (h-BN) to 29.0 at.% (mh-BN), respectively. On the other hand, the content of nitrogen and boron decreased from 45.2 at.% (h-BN) to 29.9 at.% (mh-BN) and 43.6 at.% (h-BN) to 29.4 at.% (mh-BN), indicating that the plasma removed nitrogen and boron during the plasma treatment.

**Table 1.** Chemical composition of unmodified (h-BN) and plasma-modified (h-BN50) nanoparticles obtained from XPS analysis.

Sample \ Element	N (at.%)	B (at.%)	C (at.%)	O (at.%)
h-BN	45.2	43.6	5.3	5.9
mh-BN	29.9	29.4	11.7	29.0

### 3.2. Effect of h-BN Surface Modification on Acrylic Resin Stability and Rheological Behavior

Zeta potential or Z potential measurements are a good quantitative measure to determine the stability level of acrylic resin at different concentrations of untreated and plasma-treated nanoparticles [52]. The results are shown in Table 2. Regarding the values of the zeta potential, it has been reported that values >30 mV indicate very stable positive micelles and that values <−30 mV correspond to stable values of micelles [53]. According to the zeta potential data obtained at pH = 8, the coating formulations had negative micelles in all cases. The acrylic resin showed the highest value of Z potential (−216.8 mV) due to the charges coming from the anionic stabilization of acrylic resin, which indicates its high degree of dispersion among their micelles. However, the Z potential values of the formulations with untreated nanoparticles (h-BN<sub>x</sub>) presented a considerable decrease with respect to acrylic resin (e.g., the h-BN0.1 sample presented a value of −73.5 mV), indicating that the particles disturbed the micelles of the acrylic resin due to a weak attraction between the nanoplatelet clusters and the micellar systems.

**Table 2.** Zeta potential results of the acrylic resin and the formulations with untreated (h-BN) and plasma-treated (mh-BN) nanoparticles.

Sample	Zeta Potential (mV)
Resin	−216.8
h-BN0.1	−73.5
h-BN0.5	−92.7
h-BN1	−72.6
mh-BN0.1	−130.4
mh-BN0.5	−124.4
mh-BN1	−125.3

Conversely, the potential values of the formulations with plasma-treated nanoparticles (mh-BN $x$ ) presented a slight decrease with respect to acrylic resin due to a low but better attraction with the acrylic resin emulsion, revealing the existence of greater compatibility between the h-BN50 nanoparticles with the acrylic resin micelles due to their modification with acrylic acid plasma.

In Figure 6, a scheme about the possible interactions between negative micelles of the pure latex particle is shown, with unmodified (positive charged) and modified (negative charged) h-BN nanoplatelet clusters. In Figure 6a, it can be appreciated that the positive counter-ions first wrap to the negatively charged micelle, forming the Stern layer. The micelle continues to attract more counter-ions, which could be repelled by neighbored counter-ions (diffuse layer), and by the Stern layer itself [54]. Both layers have been referred to as the double layer. The slip plane is developed where the Stern layer and diffuse layer join. The electrical potential at this point is named the zeta potential. Basically, at a higher absolute value of the zeta potential, the dispersion is more stable (particles are repelling each other). In accordance with the zeta potential value, these micelles had a highly repulsive behavior that allows the high stability of the paint. Figure 6b,c corresponds to the emulsion with mh-BN and h-BN nanoplatelets, respectively. In the case of mh-BN, the micelles had a low attraction between itself, while the h-BN had a weak attraction. Therefore, the micelles with h-BN were modified to allow for better stability between them and correspond with the zeta potential values obtained in all the concentrations.

### 3.3. Effect of h-BN Surface Modification on Viscosity Behavior

The coatings and emulsions require a complex rheology, in which the viscosity depends on the wide range of shear rate to which they are exposed during its manipulation [55]. The effect of concentration of unmodified (h-BN) and plasma-modified (mh-BN) nanoplatelets on the apparent viscosity of the acrylic resin is shown in Figure 7a. The viscosity profiles of the acrylic resin and the formulations with nanoparticles exhibited a rheological behavior of pseudoplastic type in which the viscosity value decreased as the shear rate increased [56]. The first step consisted of a constant viscosity at a low shear rate, known as the “first Newtonian plateau”, followed by a drop-in viscosity due to the shear rate exceeding the molecular relaxation of the crosslinked chains so that the viscosity was reduced. There was also a stable low viscosity at a high shear rate; this is known as the “second Newtonian plateau”, due to the Brownian movement that tries to give the original conformation to the acrylic resin molecules, but, as the shear rate continues to increase, these forces that were overcome again and continued the decrease in viscosity [56,57]. In the case of h-BN $x$  and mh-BN $x$  formulations, these samples presented a decrease in the viscosity behavior respect to the acrylic resin.

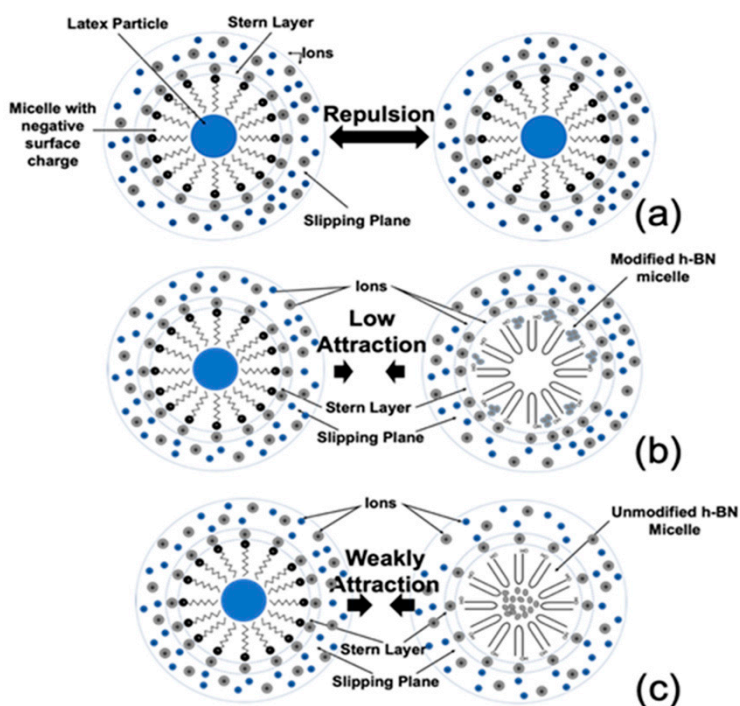


**Figure 6.** Scheme of possible Z potential behavior explanation between the different colloidal systems. (a) Emulsion (micellar) acrylic resin, (b) emulsion and modified h-BN micelle, and (c) emulsion and unmodified h-BN micelle.

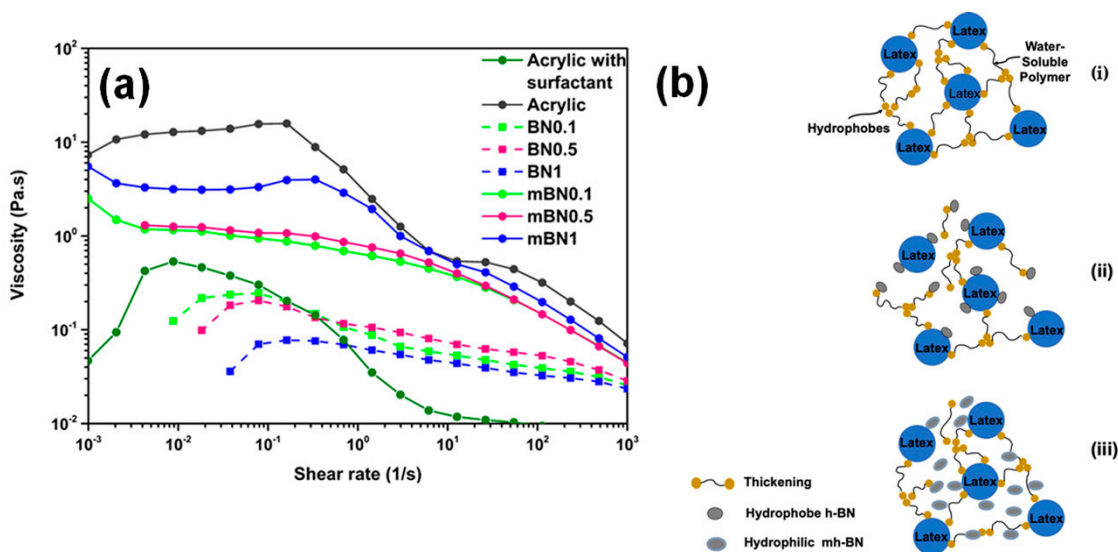


**Figure 7.** (a) Shear rheological curves of the acrylic resin and the formulations with unmodified (h-BN) and plasma-modified (mh-BN) nanoparticles, (b) the scheme of possible interactions between the latex nanoparticles, thickening and h-BN nanoparticles (i) acrylic resin (ii) acrylic coating with modified nanoplatelets and (iii) acrylic coating with unmodified nanoplatelets.

In contrast, the formulations h-BN<sub>x</sub> manifested a pronounced drop in viscosity from low to high shear rate than formulations mh-BN<sub>x</sub>. It is inferred that this behavior was due to the interruption of the weak intermolecular unions existing mainly between the unmodified nanoplatelets with the micelles of acrylic resin with the increase of the shear rate [58]. This result indicates that the modification by plasma offer to the h-BN particles better compatibility with the acrylic resin molecules and in turn improve the in-can properties.

An essential aspect to take into consideration, due to the constant growth of the market of high specialty coatings, is the degree of compatibility that exists between the different additives that structure the coatings, mainly when nanometric additives are used. [59]. Figure 7b shows a scheme with the interaction of unmodified and modified h-BN nanoplatelets with the latex and the thickening of acrylic paint. In the case of Figure 7bi, it can be appreciated that the latex is surrounded by associative thickening, which consists of a water-soluble polymer backbone that contains two or more hydrophobic groups that warranty an excellent control of the rheology and simplify the handling and the application of the coating [59,60]. In Figure 7bii,iii, it can be observed when nanoparticles are incorporated into the resin; the thickening molecules were displaced from the latex surface caused by the hydrophobic nature of the h-BN. In the case of the incorporation of mh-BN, the viscosity behavior might be due to the hydrophilic surface of these particles holding weakly interactions with the hydrophobic groups of the thickening molecules. In summary, the interactions between the latex and the h-BN can be improved by the plasma modification, which could provide a repulsion of the micelles to keep the stability on the emulsion.

### 3.4. Anticorrosive Performance of Acrylic/h-BN Coatings

Figure 8 shows the results of the impedance measurements. Figure 8a presents the Nyquist diagram for the 304-SS and the coating with the acrylic resin. In the case of 304-SS, a characteristic curve line for this type of steel is presented [61], while the acrylic resin presented two semicircles with different diameters. This behavior indicates the existence of two-time constants [62]. On the other hand, Figure 8b shows the Nyquist diagrams of nanostructured coatings with only a semicircle with different diameters. In Figure 8c, the results of the Bode-impedance show, and it is observed that 304-SS in the whole frequency range has the lowest impedance value. In the case of coatings with h-BN without treatment, it is observed that their impedance at low frequencies is slightly higher than coatings with modified nanoparticles.

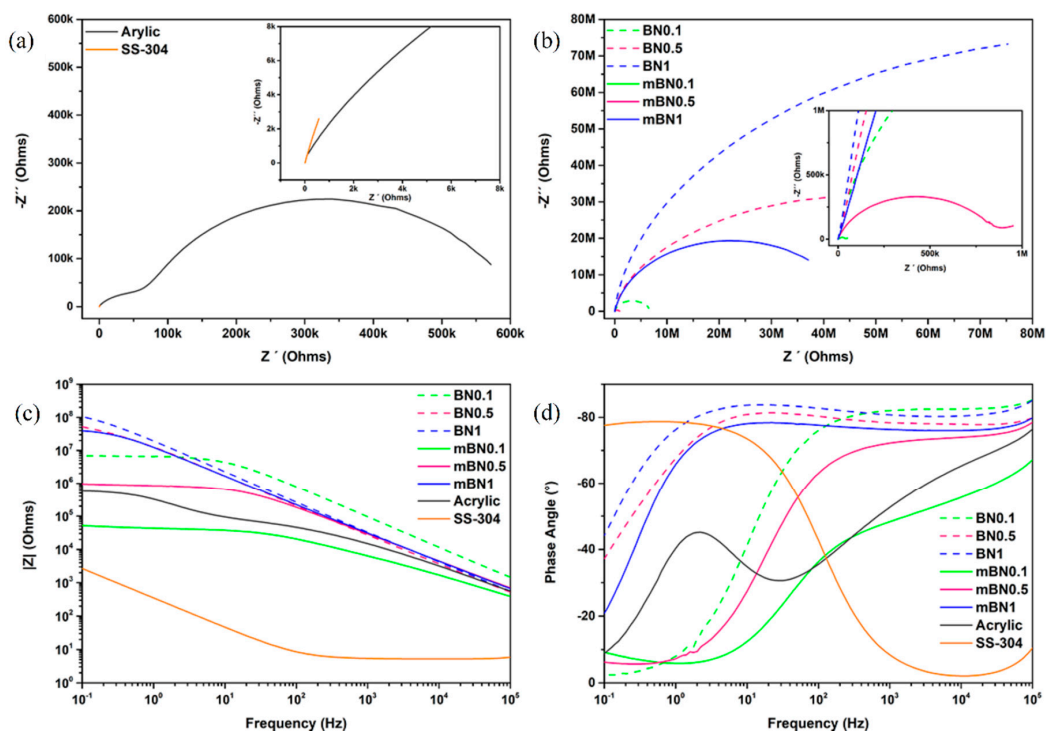


**Figure 8.** Nyquist plot for (a) acrylic resin and SS-304 and (b) formulations with nanoparticles; (c) Bode plots for phase angle vs. frequency and (d) impedance vs. frequency for different samples.

The resulting Bode-phase angle is shown in Figure 8d. It is observed that 304-SS exhibits resistive behavior at high frequencies and capacitive behavior at low frequencies. While the acrylic resin sample, showed a phase angle behavior with two-time constants, in similar form to Nyquist diagram. The appearance of two-time constants suggests that the electrolyte penetrated through the coating and reached the metal substrate, initiating the corrosion reaction of the steel. The time constant at a high-frequency range represents the characteristics of corrosion resistance or barrier properties of the coating, and the time constant at low frequencies corresponds to the properties of the coating-metal interface, that is, the controlled diffusion of the corrosion reaction [62,63].

On the contrary, all nanostructured coatings presented only a time constant, which indicates that the barrier property is improved by incorporating any of these nanoparticle systems. It was observed that for pure and modified nanoparticle coatings had the highest impedance value at low frequencies compared to acrylic resin and presented phase angles close to  $90^\circ$  in the region of high frequencies with a time constant, which represents an excellent barrier property of the coating at an initial time of immersion. It should be noted that when the concentration of the nanoparticles embedded in the acrylic resin decreased, the properties of resistance to load transfer of the coatings decreased.

Table 3 shows the results of the impedance  $|Z|$  at a low frequency that reflects the corrosive process. The impedance  $|Z|$  of all the resins is higher than the SS-304, implying a proper protection of the steel. Moreover, we can see that when increasing the h-BN content, the impedance  $|Z|$  value increases when it is not treated with plasma.

**Table 3.** Impedance  $|Z|$  at low frequency.

Sample	Impedance $ Z $ ( $\Omega\text{-cm}^2$ )
SS-304	$3.86 \times 10^4$
Resin	$8.40 \times 10^6$
h-BN0.1	$1.00 \times 10^8$
h-BN0.5	$7.49 \times 10^8$
h-BN1	$1.52 \times 10^9$
mh-BN0.1	$7.55 \times 10^5$
mh-BN0.5	$1.39 \times 10^7$
mh-BN1	$5.75 \times 10^8$

The equivalent circuits, as shown in Figure 9, were used to fit the EIS results of bare SS-304, the acrylic coating (two-time constants), and nanostructured coatings (one-time constants), respectively [21,25,64]. In the equivalent circuits,  $R_s$  was the resistance of solution, for SS-304  $R_{st}$  was the resistance of metal characteristics, and  $Q_{st}$  means the constant phase element used to simulate the capacitive response. For all the coated SS-304 samples,  $R_1$  was the resistance of the coating,  $Q_1$  was the double electrode layer capacitance of coating,  $R_2$  was the charge transfer resistance of corrosion electrochemical reaction in the metal/coating interface,  $Q_2$  was the double electrode layer capacitance in the interface and  $W$  was the impedance of Warburg associated to the diffusion phenomena of ions from the solution through the coating.

Experimental data were compared with the model, and the results are shown in Table 4, showing a good correlation between the fit to the measured data, despite the approximations made. The impedance elements of the acrylic coating suggest that the electrochemical processes might be controlled by the active species diffusing to the metal surface of corrosion products diffusing away from the metal surface through the coating film. In contrast, the acrylic/h-BN coatings maintain their high capacitive behavior. For the solution resistance, it decreases with the presence of all the coatings, mainly when the acrylic coating contained 1% of h-BN, which suggested that the coating has high superficial defects. The coating resistance ( $R_1$ ) is an important parameter that shows an increase with the content of h-BN, which results in the positive effect of these nanoparticles to incorporate into the acrylic resin. These high values of resistances show that the coating provided adequate corrosion protection. In general, when the electrolyte permeates the polymer film,  $Q_1$  may be observed to increase, which is related to an increase

in dielectric constant  $\epsilon$ , due to the increased water absorption. For  $W$  exhibits an increase while the h-BN nanoplatelets concentration increased being even higher for the modified nanoparticles, indicating that the diffusion influence of corrosive electrolyte was lower at the highest content (i.e., 1.0 wt.%) of h-BN ( $9.30 \times 10^7 \Omega/s^{(1/2)}$ ) and mh-BN ( $5.32 \times 10^8 \Omega/s^{(1/2)}$ ) [64–66]. Similar impedance spectroscopy results were recently reported for plasma-treated boron nitride nanoflakes as barriers to enhance anticorrosion of acrylic coating on steel [67], where the authors observed that the plasma modification of h-BN nanoflakes with Ar + NH<sub>3</sub> enhanced the corrosion resistance of acrylic coatings, resulting in an even a lower corrosion current density ( $I_{corr}$ ) value than pristine h-BN. This behavior was because plasma treatment can enlarge the interlayer distance and increase the formation of NH/OH groups on the h-BN surface, enhancing the storage of Fe<sup>2+</sup> ion and preventing its migration and the subsequent formation of Fe<sub>2</sub>O<sub>3</sub>.

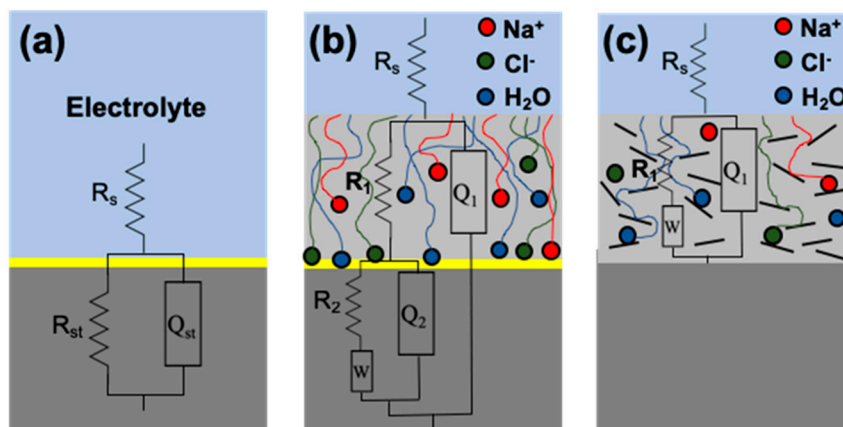


Figure 9. Electrochemical corrosion models: (a) SS-304, (b) acrylic coating and (c) nanostructured coatings.

Table 4. Electrical equivalent circuit parameters of the acrylic resin and the formulations with unmodified (h-BN) and modified treated (mh-BN) nanoparticles.

Sample	$R_s$ ( $\Omega$ )	$R_{st}$ ( $\Omega$ )	$R_1$ ( $\Omega$ )	$Q_{st}$ ( $F \cdot s^{(n_1-1)}$ )	$n_1$	$Q_1$ ( $F \cdot s^{(n_1-1)}$ )	$W$ ( $\Omega/s^{(1/2)}$ )	$R_2$ ( $\Omega$ )	$Q_2$ ( $F \cdot s^{(n_2-1)}$ )
SS-304	5.24	$6.85 \times 10^4$	–	$5.61 \times 10^{-4}$	0.886	–	–	–	–
Resin	1.31	–	$7.11 \times 10^4$	–	0.737	$9.32 \times 10^{-9}$	$1.06 \times 10^3$	$5.64 \times 10^5$	$5.16 \times 10^7$
h-BN0.1	1.10	–	$6.62 \times 10^6$	–	0.918	$3.39 \times 10^{-9}$	$2.13 \times 10^5$	–	–
h-BN0.5	0.90	–	$6.21 \times 10^7$	–	0.886	$1.54 \times 10^{-8}$	$5.68 \times 10^6$	–	–
h-BN1	0.88	–	$1.67 \times 10^8$	–	0.914	$9.97 \times 10^{-6}$	$9.30 \times 10^7$	–	–
mh-BN0.1	1.20	–	$4.39 \times 10^4$	–	0.636	$5.30 \times 10^{-7}$	$5.56 \times 10^3$	–	–
mh-BN0.5	1.10	–	$8.55 \times 10^5$	–	0.826	$2.41 \times 10^{-8}$	$7.57 \times 10^4$	–	–
mh-BN1	1.02	–	$4.93 \times 10^7$	–	0.863	$1.61 \times 10^{-8}$	$5.32 \times 10^8$	–	–

$R_s$ : resistance of solution;  $R_{st}$ : resistance of metal;  $R_1$ : resistance of coating;  $Q_{st}$ : constant phase element of metal;  $n_1$ : exponent of constant phase elements;  $Q_1$ : double electrode layer capacitance of coating;  $W$ : Impedance of Warburg;  $R_2$ : charge transfer resistance of metal/coating interface;  $Q_2$  double electrode layer capacitance at interface.

Additionally, the corrosion rate results (Table S1) corroborated the significant increase in the corrosion resistance of SS-304 ( $1.42 \times 10^{-4}$  mm/year) coated with the waterborne acrylic nanostructured coatings prepared with 0.5% and 1.0% by the weight of unmodified (h-BN) and plasma-modified (mh-BN) boron nitride nanolayers, in comparison to the pure acrylic coating ( $1.15 \times 10^{-6}$  mm/year) being the highest for the h-BN1 sample ( $4.48 \times 10^{-9}$  mm/year).

#### 4. Conclusions

In summary, h-BN nanoparticles pure and modified by plasma were used as reinforcement in acrylic matrix composite coatings. This study demonstrates that the plasma modification of the h-BN improves the dispersion and stability of the nanoplatelets, mainly at a concentration of 1% by weight, in the acrylic resin by the formation of a PAA film over the nanoplatelets’ surface, which generated electrical interactions to provide the repulsion of the micelles and keep the stability on the emulsion.

Additionally, the electrochemical studies indicate that waterborne acrylic/h-BN nanostructured coatings acted as an excellent corrosion protection of AISI 304 stainless steel. In particular, the EIS and corrosion rate results suggest that the acrylic coatings with the highest concentration (1% by weight) of pure h-BN could provide the best corrosion inhibition effect for the AISI 304 stainless steel, although the electrochemical behavior of acrylic/mh-BN nanostructured coatings, with the same nanoplatelet concentration, suggests a similar corrosion inhibition grade. Therefore, it was demonstrated that the surface modification of h-BN by plasma polymerization helped to obtain green nanostructured acrylic coatings with the right balance in in-can properties and as a barrier protection coating for the corrosion inhibition of AISI 304 stainless steel.

**Supplementary Materials:** The following are available online at <http://www.mdpi.com/2079-6412/10/5/488/s1>, Table S1: Tafel parameters for SS-304, acrylic resin and nanostructured coatings.

**Author Contributions:** Visualization, Investigation and Writing—original Draft, A.P.Y.-R.; Supervision and Conceptualization, E.H.-H.; Funding acquisition, Writing—Reviewing and Editing, G.C.-P.; Writing—Reviewing and Editing, C.A.Á.-O.; Formal Analysis, P.G.-M.; Investigation, J.A.V.-d.J.; Investigation and Formal Analysis, E.C.-D.; Investigation and Formal analysis, C.A.G.-V.; Conceptualization, Visualization, Supervision and Writing—Reviewing and Editing, J.M.M.-P. All authors have read and agreed to the published version of the manuscript.

**Funding:** This research was funded by CONACyT-SENER-Sustentabilidad Energética, Centro Mexicano de Innovación en Energía del Océano Grant No. 0249795.

**Acknowledgments:** This work was supported by the Project M-LT1 “Innovación y Desarrollo de materiales, subsistemas y componentes” from Centro Mexicano de Innovación en Energía del Océano (CEMIE-OCÉANO). We would like to thank to Alfonso Mercado, Uriel Sierra, María Guadalupe Mendez and Enrique Díaz for their assistance and expertise in physicochemical and structural (TEM) characterization testing.

**Conflicts of Interest:** The authors declare no conflict of interest.

## References

1. Huang, G.; Qu, L.; Lu, Y.; Wang, Y.; Li, H.; Qin, Z.; Lu, X. Corrosion resistance improvement of 45 steel by Fe-based amorphous coating. *Vacuum* **2018**, *153*, 39–42. [[CrossRef](#)]
2. Koch, G.H.; Thompson, N.G.; Moghissi, O.; Payer, J.H.; Varney, J. *IMPACT (International Measures of Prevention, Application, and Economics of Corrosion Technologies Study)*; Report No. OAPUS310GKCOCH (AP110272); NACE International: Houston, TX, USA, 2016.
3. Cui, M.; Ren, S.; Chen, J.; Liu, S.; Zhang, G.; Zhao, H.; Wang, L.; Xue, Q. Anticorrosive performance of waterborne epoxy coatings containing water-dispersible hexagonal boron nitride (h-BN) nanosheets. *Appl. Surf. Sci.* **2017**, *397*, 77–86. [[CrossRef](#)]
4. Li, J.; Yao, C.; Liu, Y.; Li, D.; Zhou, B.; Cai, W. The hazardous hexavalent chromium formed on trivalent chromium conversion coating: The origin, influence factors and control measures. *J. Hazard. Mater.* **2012**, *221*, 56–61. [[CrossRef](#)] [[PubMed](#)]
5. Alzieu, C. Tributyltin: Case study of a chronic contaminant in the coastal environment. *Ocean Coast. Manag.* **1998**, *40*, 23–36. [[CrossRef](#)]
6. Oliveira, R.; Gonçalves, J.; Ueda, M.; Oswald, S.; Baldissera, S. Improved corrosion resistance of tool steel H13 by means of cadmium ion implantation and deposition. *Surf. Coat. Technol.* **2010**, *204*, 2981–2985. [[CrossRef](#)]
7. Wu, B.; Lu, S.; Xu, W.; Cui, S.; Li, J.; Han, P. Study on corrosion resistance and photocatalysis of cobalt superhydrophobic coating on aluminum substrate. *Surf. Coat. Technol.* **2017**, *330*, 42–52. [[CrossRef](#)]
8. Chasse, K.R.; Scardino, A.J.; Swain, G.W. Corrosion and fouling study of copper-based antifouling coatings on 5083 aluminum alloy. *Prog. Org. Coat.* **2020**, *141*, 105555. [[CrossRef](#)]
9. Nine, J.; Cole, M.A.; Tran, D.N.H.; Losic, D. Graphene: A multipurpose material for protective coatings. *J. Mater. Chem. A* **2015**, *3*, 12580–12602. [[CrossRef](#)]
10. Nguyen, T.V.; Tri, P.N.; Nguyen, T.D.; El Aidani, R.; Trinh, V.T.; Decker, C. Accelerated degradation of water borne acrylic nanocomposites used in outdoor protective coatings. *Polym. Degrad. Stab.* **2016**, *128*, 65–76. [[CrossRef](#)]
11. Mariz, I.F.A.; Millichamp, I.S.; de la Cal, J.C.; Leiza, J.R. High performance water-borne paints with high volume solids based on bimodal latexes. *Prog. Org. Coat.* **2010**, *68*, 225–233. [[CrossRef](#)]

12. Karger-Kocsis, J. Paints, coatings and solvents. *Compos. Sci. Technol.* **1994**, *51*, 613–614. [[CrossRef](#)]
13. Forsgren, A. *Corrosion Control Through Organic Coatings*, 1st ed.; Corrosion Technology; CRC Press, Taylor & Francis Group: Boca Raton, FL, USA, 2006; pp. 55–57. ISBN 978-0-8493-7278-0.
14. Yu, F.; Xu, X.; Lin, N.; Liu, X.Y. Structural engineering of waterborne polyurethane for high performance waterproof coatings. *RSC Adv.* **2015**, *5*, 72544–72552. [[CrossRef](#)]
15. Kugler, S.; Kowalczyk, K.; Spychaj, T. Influence of dielectric nanoparticles addition on electroconductivity and other properties of carbon nanotubes-based acrylic coatings. *Prog. Org. Coat.* **2016**, *92*, 66–72. [[CrossRef](#)]
16. Wang, N.; Fu, W.; Sun, M.; Zhang, J.; Fang, Q. Effect of different structured TiO<sub>2</sub> particle on anticorrosion properties of waterborne epoxy coatings. *Corros. Eng. Sci. Technol.* **2016**, *51*, 365–372. [[CrossRef](#)]
17. Palimi, M.J.; Rostami, M.; Mahdavian, M.; Ramezanzadeh, B.; Mahdavian, M. A study on the corrosion inhibition properties of silane-modified Fe<sub>2</sub>O<sub>3</sub> nanoparticle on mild steel and its effect on the anticorrosion properties of the polyurethane coating. *J. Coat. Technol. Res.* **2015**, *12*, 277–292. [[CrossRef](#)]
18. Ates, M. A review on conducting polymer coatings for corrosion protection. *J. Adhes. Sci. Technol.* **2016**, *30*, 1–27. [[CrossRef](#)]
19. Dennis, R.V.; Patil, V.; Andrews, J.; Aldinger, J.P.; Yadav, G.D.; Banerjee, S. Hybrid nanostructured coatings for corrosion protection of base metals: A sustainability perspective. *Mater. Res. Express* **2015**, *2*, 32001. [[CrossRef](#)]
20. Olajire, A.A. Recent advances on organic coating system technologies for corrosion protection of offshore metallic structures. *J. Mol. Liq.* **2018**, *269*, 572–606. [[CrossRef](#)]
21. Li, J.; Gan, L.; Liu, Y.; Mateti, S.; Lei, W.; Chen, Y.; Yang, J. Boron nitride nanosheets reinforced waterborne polyurethane coatings for improving corrosion resistance and antifriction properties. *Eur. Polym. J.* **2018**, *104*, 57–63. [[CrossRef](#)]
22. Cui, M.; Ren, S.; Qin, S.; Xue, Q.; Zhao, H.; Wang, L. Non-covalent functionalized hexagonal boron nitride nanoplatelets to improve corrosion and wear resistance of epoxy coatings. *RSC Adv.* **2017**, *7*, 44043–44053. [[CrossRef](#)]
23. Yu, Y.-H.; Lin, Y.-Y.; Lin, C.-H.; Chan, C.-C.; Huang, Y.-C. High-performance polystyrene/graphene-based nanocomposites with excellent anti-corrosion properties. *Polym. Chem.* **2014**, *5*, 535–550. [[CrossRef](#)]
24. Günthner, M.; Kraus, T.; Krenkel, W.; Motz, G.; Dierdorf, A.; Decker, D. Particle-filled PHPS silazane-based coatings on steel. *Int. J. Appl. Ceram. Technol.* **2009**, *6*, 373–380. [[CrossRef](#)]
25. Husain, E.; Narayanan, T.N.; Taha-Tijerina, J.; Vinod, S.; Vajtai, R.; Ajayan, P.M. Marine corrosion protective coatings of hexagonal boron nitride thin films on stainless steel. *ACS Appl. Mater. Interfaces* **2013**, *5*, 4129–4135. [[CrossRef](#)] [[PubMed](#)]
26. Hernández-Hernández, E.; Neira-Velázquez, M.; Valle, L.R.-D.; Ponce, A.; Weinkauff, D. Changing the surface characteristics of CNF, from hydrophobic to hydrophilic, via plasma polymerization with acrylic acid. *J. Nano Res.* **2010**, *9*, 45–53. [[CrossRef](#)]
27. Ramos-Devalle, L.F.; Neira-Velázquez, M.G.; Hernández-Hernández, E. Surface modification of CNFs via plasma polymerization of styrene monomer and its effect on the properties of PS/CNF nanocomposites. *J. Appl. Polym. Sci.* **2007**, *107*, 1893–1899. [[CrossRef](#)]
28. Neira-Velázquez, M.G.; Borjas-Ramos, J.; Hernández-Hernández, E.; Hernández-Ramos, C.G.; Narro-Céspedes, R.I.; Hernández-Gámez, J.F.; De Valle, L.F.R. Nanocomposites Prepared with high density polyethylene and carbon nanofibers modified by ethylene plasma. *Plasma Process. Polym.* **2015**, *12*, 477–485. [[CrossRef](#)]
29. Neira-Velázquez, M.G.; Ramos-De Valle, L.F.; Hernández-Hernández, E.; Pedraza, A.P.; Solís-Rosales, S.G.; Sánchez-Valdez, S.; Bartolo-Pérez, P.; Gonzalez-Gonzalez, V.A. Surface modification of nanoclays by plasma polymerization of ethylene. *Plasma Process. Polym.* **2011**, *8*, 842–849. [[CrossRef](#)]
30. Solís-Gómez, A.; Neira-Velázquez, M.G.; Morales, J.; Sánchez-Castillo, M.A.; Perez, E. Improving stability of TiO<sub>2</sub> particles in water by RF-plasma polymerization of poly(acrylic acid) on the particle surface. *Colloids Surfaces A: Physicochem. Eng. Asp.* **2014**, *451*, 66–74. [[CrossRef](#)]
31. Navarro-Rosales, M.; Ávila-Orta, C.A.; Neira-Velázquez, M.G.; Ortega-Ortíz, H.; Hernández-Hernández, E.; Solís-Rosales, S.G.; Sánchez, B.L.E.; González-Morones, P.; Jiménez, R.; Sánchez-Valdes, S.; et al. Effect of plasma modification of copper nanoparticles on their antibacterial properties. *Plasma Process. Polym.* **2014**, *11*, 685–693. [[CrossRef](#)]

32. Covarrubias-Gordillo, C.A.; Corral, F.S.; Ávila-Orta, C.A.; Cruz-Delgado, V.; Neira-Velázquez, M.G.; Hernández-Hernández, E.; Hernández-Gómez, J.F.; De León-Martínez, P.A. Surface modification of carbon nanofibers and graphene platelets mixtures by plasma polymerization of propylene. *J. Nanomater.* **2017**, *2017*, 1–10. [[CrossRef](#)]
33. Cho, D.-H.; Kim, J.-S.; Kwon, S.-H.; Lee, C.; Lee, Y.-Z. Evaluation of hexagonal boron nitride nano-sheets as a lubricant additive in water. *Wear* **2013**, *302*, 981–986. [[CrossRef](#)]
34. Lin, Y.; Williams, T.; Xu, T.-B.; Cao, W.; Elsayed-Ali, H.E.; Connell, J.W. Aqueous dispersions of few-layered and monolayered hexagonal boron nitride nanosheets from sonication-assisted hydrolysis: Critical role of water. *J. Phys. Chem. C* **2011**, *115*, 2679–2685. [[CrossRef](#)]
35. Duan, J.; Xue, R.; Xu, Y.; Sun, C. Low temperature synthesis of h-BN nanoflakes. *Mater. Lett.* **2008**, *62*, 3355–3357. [[CrossRef](#)]
36. Singla, P.; Goel, N.; Kumar, V.; Singhal, S. Boron nitride nanomaterials with different morphologies: Synthesis, characterization and efficient application in dye adsorption. *Ceram. Int.* **2015**, *41*, 10565–10577. [[CrossRef](#)]
37. Kostoglou, N.; Polychronopoulou, K.; Rebholz, C. Thermal and chemical stability of hexagonal boron nitride (h-BN) nanoplatelets. *Vacuum* **2015**, *112*, 42–45. [[CrossRef](#)]
38. Petisco-Ferrero, S.; Sánchez-Ilárduya, M.B.; Díez, A.; Martín, L.; Meaurio Arrate, E.; Sarasua, J.R. Surface functionalization of an osteoconductive filler by plasma polymerization of poly( $\epsilon$ -caprolactone) and poly(acrylic acid) films. *Appl. Surf. Sci.* **2016**, *386*, 327–336. [[CrossRef](#)]
39. Lu, X.; Tan, C.Y.; Xu, J.; He, C. Thermal degradation of electrical conductivity of polyacrylic acid doped polyaniline: Effect of molecular weight of the dopants. *Synth. Met.* **2003**, *138*, 429–440. [[CrossRef](#)]
40. Sheng, L.; Huang, S.; Sui, M.; Zhang, L.; She, L.; Chen, Y. Deposition of copper nanoparticles on multiwalled carbon nanotubes modified with poly (acrylic acid) and their antimicrobial application in water treatment. *Front. Environ. Sci. Eng.* **2014**, *9*, 625–633. [[CrossRef](#)]
41. Shi, Y.; Hamsen, C.; Jia, X.; Kim, K.K.; Reina, A.; Hofmann, M.; Hsu, A.L.; Zhang, K.; Li, H.; Juang, Z.-Y.; et al. Synthesis of few-layer hexagonal boron nitride thin film by chemical vapor deposition. *Nano Lett.* **2010**, *10*, 4134–4139. [[CrossRef](#)]
42. Nocua, J.E.; Morell, G.; Piazza, F.; Weiner, B.R. Síntesis y caracterización de nanoestructuras estequiométricas de nitruro de boro. *Superf. y Vacío* **2012**, *25*, 194–198.
43. Borjas-Ramos, J.; Ramos-De Valle, L.F.; Velázquez, M.G.N.; Hernández-Hernández, E.; Saucedo-Salazar, E.M.; Soria, G. Thermal conductivity of nanocomposites based in high density polyethylene and surface modified hexagonal boron nitride via cold ethylene plasma. *Plasma Chem. Plasma Process.* **2017**, *38*, 429–441. [[CrossRef](#)]
44. Achour, H.; Achour, A.; Solaymani, S.; Islam, M.; Vizireanu, S.; Arman, A.; Ahmadpourian, A.; Dinescu, G. Plasma surface functionalization of boron nitride nano-sheets. *Diam. Relat. Mater.* **2017**, *77*, 110–115. [[CrossRef](#)]
45. Huang, C.; Liu, Q.; Fan, W.; Qiu, X. Boron nitride encapsulated copper nanoparticles: A facile one-step synthesis and their effect on thermal decomposition of ammonium perchlorate. *Sci. Rep.* **2015**, *5*, 16736. [[CrossRef](#)] [[PubMed](#)]
46. Qiu, X.; Wu, X.; Liu, Q.; Huang, C. The release of hydrogen from ammonia borane over copper/hexagonal boron nitride composites. *RSC Adv.* **2016**, *6*, 106211–106217. [[CrossRef](#)]
47. Sudeep, P.M.; Vinod, S.; Sruthi, R.; Anantharaman, M.R.; Ozden, S.; Kukovecz, Á.; Kónya, Z.; Vajtai, R.; Ajayan, P.M.; Narayanan, T.N. Functionalized boron nitride porous solids. *RSC Adv.* **2015**, *5*, 93964–93968. [[CrossRef](#)]
48. Hernandez-Hernandez, E. *Funcionalización de Nanopartículas por Plasma y su Efecto en las Propiedades de Nanocompuestos Poliméricos*; Centro de Investigación en Química Aplicada: Saltillo, Mexico, 2011.
49. O'Toole, L.; Beck, A.J.; Short, R.D. Characterization of plasma polymers of acrylic acid and propanoic acid. *Macromolecules* **1996**, *29*, 5172–5177. [[CrossRef](#)]
50. Lan, Y.; You, Q.; Cheng, C.; Zhang, S.; Ni, G.; Meng, Y. Graft polymerization of acrylic acid on a polytetrafluoroethylene panel by an inductively coupled plasma. *Plasma Sci. Technol.* **2011**, *13*, 88–92. [[CrossRef](#)]
51. Jarvis, K.; McArthur, S. Exploiting reactor geometry to manipulate the properties of plasma polymerized acrylic acid films. *Materials* **2019**, *12*, 2597. [[CrossRef](#)] [[PubMed](#)]
52. Zhi, C.; Xu, Y.; Bando, Y.; Golberg, D. Highly thermo-conductive fluid with boron nitride nanofillers. *ACS Nano* **2011**, *5*, 6571–6577. [[CrossRef](#)]

53. Prieto García, F.; Prieto Méndez, J.; de Ita Gutiérrez, S.; Méndez Marzo, M.A.; Román Gutiérrez, A.D. Correlación de Potencial Zeta y Parámetros Físicoquímicos en Extractos de Saturación de Suelos del Distrito de Riego-03, Valle del Mezquital, Hidalgo, México. *Trop. Subtrop. Agroecosystems* **2009**, *10*, 161–167.
54. Cho, D.; Lee, S.; Frey, M.W. Characterizing zeta potential of functional nanofibers in a microfluidic device. *J. Colloid Interface Sci.* **2012**, *372*, 252–260. [[CrossRef](#)]
55. Yilmaz, O.; Cheaburu, C.N.; Gülümser, G.; Vasile, C. Rheological behaviour of acrylate/montmorillonite nanocomposite latexes and their application in leather finishing as binders. *Prog. Org. Coat.* **2011**, *70*, 52–58. [[CrossRef](#)]
56. De Oliveira, A.R.; Abrishamkar, A.; Veloso, E.M.; De Oliveira, F.C.; Da Silva, J.G.; Pereira, J.R.; Diniz, L.F.; Denadai, Â.M.L. Effect of composition on rheological behavior of iron oxides produced by hydrothermal method. *Ceram. Int.* **2017**, *43*, 7436–7442. [[CrossRef](#)]
57. Zolper, T.J.; Seyam, A.M.; Chen, C.; Jungk, M.; Stammer, A.; Stoegbauer, H.; Marks, T.J.; Chung, Y.-W.; Wang, Q. Energy efficient siloxane lubricants utilizing temporary shear-thinning. *Tribol. Lett.* **2013**, *49*, 525–538. [[CrossRef](#)]
58. Wu, Z.; Wu, J.; Zhang, R.; Yuan, S.; Lu, Q.; Yu, Y. Colloid properties of hydrophobic modified alginate: Surface tension,  $\zeta$ -potential, viscosity and emulsification. *Carbohydr. Polym.* **2018**, *181*, 56–62. [[CrossRef](#)] [[PubMed](#)]
59. Saucy, D. Avoiding Viscosity Loss on Tinting. *Paint Coat. Ind.* **2008**, *24*, 34–38.
60. Bhavsar, R.A.; Nehete, K.M. Rheological approach to select most suitable associative thickener for water-based polymer dispersions and paints. *J. Coat. Technol. Res.* **2019**, *16*, 1089–1098. [[CrossRef](#)]
61. Román, A.S.; Barrientos, M.S.; Harms, F.; Marcelamendez, C.; Estherares, A. Resistencia corrosión de acero inoxidable AISI 304L en biodiesel de soja corrosion resistance of AISI 304L stainless steel in soybean biodiesel. *An. Afa* **2016**, *271*, 14–18. [[CrossRef](#)]
62. Ruhi, G.; Modi, O.; Dhawan, S. Chitosan-poly pyrrole-SiO<sub>2</sub> composite coatings with advanced anticorrosive properties. *Synth. Met.* **2015**, *200*, 24–39. [[CrossRef](#)]
63. Pakdel, A.; Zhi, C.; Bando, Y.; Nakayama, T.; Golberg, D. Boron nitride nanosheet coatings with controllable water repellency. *ACS Nano* **2011**, *5*, 6507–6515. [[CrossRef](#)]
64. Liang, J.; Srinivasan, P.B.; Blawert, C.; Dietzel, W. Comparison of electrochemical corrosion behaviour of MgO and ZrO<sub>2</sub> coatings on AM50 magnesium alloy formed by plasma electrolytic oxidation. *Corros. Sci.* **2009**, *51*, 2483–2492. [[CrossRef](#)]
65. Mishra, M.K.; Gunasekaran, G.; Rao, A.G.; Kashyap, B.P.; Prabhu, N. Effect of multipass friction stir processing on mechanical and corrosion behavior of 2507 super duplex stainless steel. *J. Mater. Eng. Perform.* **2016**, *26*, 849–860. [[CrossRef](#)]
66. Sah, S.P. Corrosion of 304 stainless steel in carbonates melt—A state of enhanced dissolution of corrosion products. *Corros. Sci.* **2020**, *169*, 108535. [[CrossRef](#)]
67. Zou, B.; Chang, X.; Yang, J.; Wang, S.; Xu, J.; Wang, S.; Samukawa, S.; Wang, L. Plasma treated h-BN nanoflakes as barriers to enhance anticorrosion of acrylic coating on steel. *Prog. Org. Coat.* **2019**, *133*, 139–144. [[CrossRef](#)]

